

# Optimization of Rate-Splitting Multiple Access with Integrated Sensing and Backscatter Communication

Diluka Galappaththige, *Member, IEEE*, Shayan Zargari, Chintha Tellambura, *Fellow, IEEE*, and Geoffrey Ye Li, *Fellow, IEEE*,

**Abstract**—An integrated sensing and backscatter communication (ISABC) system is introduced herein. This system features a full-duplex (FD) base station (BS) that seamlessly merges sensing with backscatter communication and supports multiple users. Multiple access (MA) for the user is provided by employing rate-splitting multiple access (RSMA). RSMA, unlike other classical orthogonal and non-orthogonal MA schemes, splits messages into common and private streams. With RSMA, the set of common rate forms can be optimized to reduce interference. Optimized formulas are thus derived for communication rates for users, tags, and the BS’s sensing rate, with the primary goal of enhancing the transmission efficiency of the BS. The optimization task involves minimizing the BS’s overall transmission power by jointly optimizing the BS’s beamforming vectors, the tag reflection coefficients, and user common rates. The alternating optimization method is employed to address this challenge. Concrete solutions are provided for the received beamformers, and semi-definite relaxation and slack-optimization techniques are adopted for transmit beamformers and reflection coefficients, respectively. For example, the proposed RSMA-assisted ISABC system achieves a 350% communication rate boost over a non-orthogonal multiple access-assisted ISABC, with only a 24% increase in transmit power, leveraging ten transmit/reception antennas at the BS.

**Index Terms**—Backscatter communication (BackCom), integrated sensing and communication (ISAC), passive tags, rate-splitting multiple access (RSMA).

## I. INTRODUCTION

Integrated sensing and communications (ISAC) networks are envisioned for 6G wireless. In traditional radar-based sensing, a reflected signal from an object/target is used to sense/detect the object [1]. Similarly, backscatter communication (BackCom) uses radar-like load modulation to send data, i.e., a backscatter device (or a tag) modulates its data onto an external radio frequency (RF) signal and reflects it to a reader [2]–[5]. However, all the existing ISAC works do not consider backscatter scenarios, except for [6], [7]. In [6], by leveraging the similarities between BackCom and radar systems, i.e., the use of reflected signals, a novel concept called *Integrated Sensing and Backscatter Communications (ISABC)*, has been proposed. This work investigates the feasibility of integrating sensing into low-power Internet-of-Things (IoT) devices. This new paradigm combines integrated sensing and communication (ISAC) with BackCom features, resulting in concurrent sensing and communication in ambient power-enabled IoT networks.

D. Galappaththige, S. Zargari, and C. Tellambura with the Department of Electrical and Computer Engineering, University of Alberta, Edmonton, AB, T6G 1H9, Canada (e-mail: {diluka.lg, zargari, ct4}@ualberta.ca).

G. Y. Li is with the ITP Lab, the Department of Electrical and Electronic Engineering, Imperial College London, SW7 2BX London, U.K. (e-mail: geoffrey.li@imperial.ac.uk).

TABLE I: A comparison between ISAC and ISABC.

Features	ISAC	ISABC
Target	✓	×
Tag	×	✓
Additional user data	×	✓
BS Power allocation	✓	✓
User decoding	Conventional	SIC
Sensing type	Active/Passive	Active

Combining the strengths of ISAC and BackCom, ISABC introduces backscatter tags as replacements for the conventional sensing targets, enabling opportunistic sensing in BackCom systems [6]. Although ISABC belongs to devices-based ISAC with active sensing, this modification distinguishes ISABC from traditional ISAC in several significant ways (Table I).

In ISAC, sensing targets can be passive objects, such as vehicles, which neither transmit nor receive sensing signals, nor active devices, such as mobile phones, which engage in transmitting and/or receiving. In contrast, ISABC pivots around backscatter tags acting as sensing targets. These tags relay environmental details to the base station (BS) and transmit additional data to users or readers. For example, in a smart home, tags can be deployed to monitor and map surroundings. Thus, the BS can use the tag-reflected signals for sensing. This approach enhances communication and sensing capabilities by harnessing both sensing and backscatter data. However, the user/reader may need more advanced decoding mechanisms, such as successive interference cancellation (SIC).

Applications of ISABC may include the following. For example, emerging IoT networks demand highly accurate and robust sensing, high data throughput, low latency, connectivity, reliability, and energy efficiency [8], [9]. Specifically, ambient power-enabled (i.e., battery-free) IoT is a key contender for applications like smart homes, smart cities, industrial IoT, and more, which require sensing, collecting, and exchanging data about the environment without requiring explicit human input or control [2]–[4]. Moreover, BackCom-aided vehicular networks for navigation, traffic monitoring, pedestrian monitoring, environmental surveillance, road safety, and autonomous driving demand sensing capabilities [10], [11]. Thus, ISABC can facilitate sensing requirements for such applications.

This research thus extends the notion of [6], [7] to a general framework with enhanced spectrum efficiency by integrating it with rate-splitting multiple access (RSMA) (see Section I-B).

### A. ISAC, RSMA, and BackCom

Since our study integrates these three technologies, this section briefly describes them.

ISAC aims to reshape sixth-generation (6G) networks, significantly shifting from traditional network architectures. It en-

ables services such as localization, activity monitoring, object detection, and environmental mapping. Conversely, ISAC can enhance communication performance by using environmental data to provide precise beamforming, rapid beam failure recovery, and reduced channel estimation overhead [12].

Two main ISAC categories are [12]: (i) Device-free ISAC and (ii) Device-based ISAC. The first refers to detecting unregistered external targets, such as vehicles, animals, and humans, making the sensing approach independent of the targets' transmission and/or reception capability. In device-based ISAC, network-registered devices, such as mobile phones and IoT sensors, provide sensing functionality, resulting in a target transmission and/or reception-based sensing approach. These categories can further be subdivided according to the transmitter and receiver configurations (i.e., mono-, bi-, and multi-static), as well as the type of sensing signal (i.e., active if the sensing receiver uses its transmit signals or passive if it uses external sensing signals) [12]. Active sensing employs full-duplex (FD) mode, which affects sensing performance due to self-interference (SI) [13]. However, an FD ISAC system must only perform IS cancellation for direct signal coupling between transceiver antennas while keeping target reflections. Fortunately, machine learning-based cancellation, digital cancellation, analog cancellation, and antenna isolation can successfully suppress the SI [14].

RSMA has recently emerged as a viable multiple-access scheme with effective interference control [15]–[17]. It relies on splitting user messages into multiple parts and allowing for partial decoding of interference and partial treatment of interference as noise [15]–[17]. In particular, RSMA divides each user's message into a common part and a private part, with the common parts of all users encoded into a single common stream and the private part encoded individually. Before decoding the corresponding private stream, each user decodes and removes the common stream via SIC. RSMA offers superior spectrum and energy efficiencies than other conventional multiple access schemes, such as space-division multiple access (SDMA), which regards interference as noise, and non-orthogonal multiple access (NOMA), which decodes interference [15]–[17].

BackCom is a promising avenue for facilitating energy-efficient IoT networks [2]–[4]. It enables wireless nodes (tags or IoT devices) to communicate by reflecting external radio frequency (RF) signals. Thus, tags can operate without active RF components. This approach may be a sustainable alternative for battery-dependent IoT devices, which incur high maintenance costs, environmental impact, and safety issues [2]–[4]. These tags, without active RF components and reflecting external RF, achieve ultra-low cost and energy use, ranging from nanowatts to microwatts [2].

### B. Motivation and Our Contribution

This study introduces a novel and generalized system model for ISABC: multiple tags, multiple users, a backscatter reader, and an FD BS (Fig. 1). This network combines primary users, tags, a reader, and sensing into a unified framework, posing three critical challenges.

- 1) The first challenge is the provision of multiple access for primary users. Conventional options include time-division multiple access (TDMA), NOMA, and SDMA. SDMA treats all undesired signals as interference, which saturates the rates even with excess transmit powers if the number of transmit antennas is insufficient or a resource block has multiple users [18]. In contrast, by employing superposition coding and SIC, NOMA can serve multiple users over the same resource block. However, the drawbacks are that NOMA has stringent decoding and SIC requirements and that channel gains must have a significant disparity [18]. RSMA outperforms these regarding spectrum and energy efficiencies [18]. Due to these reasons, RSMA is proposed in this study and is evaluated against NOMA and SDMA benchmarks.
- 2) The second challenge is for the reader to detect the tag signals significantly weaker than direct signals due to the double path loss effect [2]–[4]. Before decoding the tags' data, the reader must reduce direct link interference (DLI) [19]. While the reader and BS can be connected, DLI cannot be eliminated due to the reader's limited dynamic range. The reader thus employs imperfect SIC to partially remove DLI before decoding the backscatter data [19].
- 3) The third challenge is the BS's ability to sense the tag signals, while strong SI affects its sensing [13]. To successfully sense the tag-reflected signal, the BS must reduce SI power to a level comparable to the tags' backscattered signal power [13]. The SI suppression is not perfect. Thus, the BS will operate with a residual SI.

Prior works [6] and [7] have several limitations. Specifically, [6] considers only one backscatter tag and a user, a special case of our model (Fig. 1). Thus, [6] does not consider multiple access for users. Reference [7] extends [6] for multiple tags and a single user. However, it uses perfect SIC for backscatter data decoding at the user and perfect SI cancellation at the BS for acquiring sensing information. Conversely, this work generalizes the system model and addresses the technical limitations in [6], [7] by investigating multi-tag with EH, RSMA-enabled multiple access for the primary users, and effects of imperfect SIC and SI cancellation. Thus, the optimization framework differs radically from [7].

Inspired by the aforementioned challenges and potential applications of ISABC, we present a novel RSMA-enabled ISABC system. Our contributions are summarized as follows:

- 1) Utilizing RSMA, the BS facilitates multiple access for the primary users to enhance the primary communication performance. The tags reflect the BS's signal to communicate with the reader, while the BS uses the same reflected signal to infer the tags' environmental insights.
- 2) The BS transmit power is minimized while preserving quality-of-service (QoS) requirements for all nodes, including tags and users. The optimization variables are the BS transmit/received beamforming, tag reflection coefficients, and users' common rates. Due to the appearance of the products of the optimization variables, the proposed problem  $\mathbf{P}_1$  (17) is non-convex, and the widely available convex algorithms fail to solve it.

- 3) To address this, an alternative optimization (AO) strategy [20] is employed, beginning by optimizing the BS received beamforming for the tags' signal using minimum mean-squared error (MMSE) filtering and the generalized Rayleigh quotient form of the signal-to-noise-to-interference ratio (SINR). The semidefinite relaxation (SDR) approach is then used to determine the BS transmit beamforming and the user common rates [21], [22]. Finally, the feasibility problem of tag reflection coefficient optimization is transformed into a slack-optimization problem to obtain an effective solution [23], [24].
- 4) The benefits of the proposed RSMA-assisted ISABC are compared to NOMA-assisted ISABC, RSMA-assisted BackCom, conventional BackCom, conventional ISABC, and sensing-only schemes (with energy harvesting (EH)). The convergence and complexity are also analyzed. With a configuration of ten BS antennas each for transmission and reception, the proposed scheme offers a 350% communication rate enhancement compared to the NOMA-assisted ISABC while only necessitating a modest 24% transmit power rise.

*Notation:* Boldface lower case and upper case letters represent vectors and matrices, respectively. For matrix  $\mathbf{A}$ ,  $\mathbf{A}^H$  and  $\mathbf{A}^T$  are Hermitian conjugate transpose and transpose of matrix  $\mathbf{A}$ , respectively.  $\mathbf{I}_M$  denotes the  $M$ -by- $M$  identity matrix. The Euclidean norm, absolute value, and expectation operators are denoted by  $\|\cdot\|$  and  $|\cdot|$ , and  $\mathbb{E}\{\cdot\}$ , respectively. A circularly symmetric complex Gaussian (CSCG) random vector with mean  $\boldsymbol{\mu}$  and covariance matrix  $\mathbf{C}$  is denoted by  $\sim \mathcal{CN}(\boldsymbol{\mu}, \mathbf{C})$ . Besides,  $\mathbb{C}^{M \times N}$  and  $\mathbb{R}^{M \times 1}$  represent  $M \times N$  dimensional complex matrices and  $M \times 1$  dimensional real vectors, respectively. Further,  $\mathcal{O}$  expresses the big-O notation. Finally,  $\mathcal{L} \triangleq \{1, \dots, L\}$ ,  $\mathcal{K} \triangleq \{1, \dots, K\}$ ,  $\mathcal{L}_l \triangleq \mathcal{L} \setminus \{l\}$ ,  $\mathcal{K}_k \triangleq \mathcal{K} \setminus \{k\}$ ,  $\mathcal{L}'_l \triangleq \{1, \dots, l-1\}$ , and  $\mathcal{L}''_l \triangleq \{l+1, \dots, L\}$ .

## II. SYSTEM COMPONENTS

### A. System Model

An RSMA-assisted ISABC system (Fig. 1) is considered. It consists of an FD BS as the primary transmitter having  $M$  transmit and  $N$  receiver uniform linear array (ULA) antennas,  $L$  single-antenna users ( $U_l$  denotes the  $l$ -th user),  $K$  single-antenna tags ( $T_k$  denotes the  $k$ -th tag), and a single-antenna reader. The BS antennas are spaced at half-wavelengths [13]. Tags use power-splitting (PS) protocol for EH and data backscattering (Section II-D).

The BS communicates and senses the surroundings using transmit beamforming, whereas tags use the BS signal for EH and data backscattering via the PS protocol. Cooperation is assumed between the BS and the backscatter reader via a control link [25]. Thus, the reader subtracts the direct signal, i.e.,  $\mathbf{f}_0 \mathbf{x}$ , from its received signal before decoding the tag data. This SIC operation minimizes the interference from the BS. The BS also extracts environmental insights from unintentionally received backscatter signals [6]. To reduce self-interference (SI), the BS uses two distinct antenna sets for transmission and reception [13]. Time synchronization of the nodes is assumed for simplicity [19].

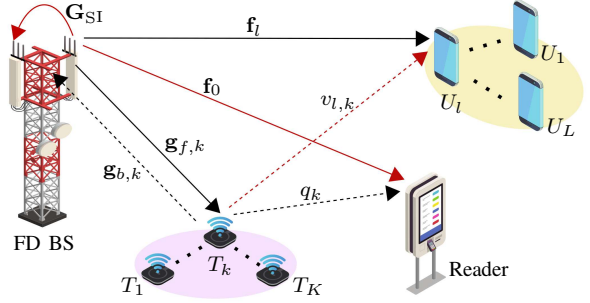


Fig. 1: An RSMA-assisted ISABC system setup. Red lines denote interference links.

### B. Channel Model

This study employs block flat-fading channel models. During each fading block,  $\mathbf{f}_0 \in \mathbb{C}^{M \times 1}$ ,  $\mathbf{f}_l \in \mathbb{C}^{M \times 1}$ , and  $\mathbf{g}_{f,k} \in \mathbb{C}^{M \times 1}$ , respectively, represent the channels between the BS and the reader, the BS and  $U_l$ , and the BS and  $T_k$ . The channels between  $T_k$  and  $U_l$ , and  $T_k$  and the reader are denoted by  $v_{l,k}$  and  $q_k$ , respectively, while  $\mathbf{g}_{b,k} \in \mathbb{C}^{N \times 1}$  represents the channel between  $T_k$  and the BS receiver antennas. Within these channels, pure communication channels, i.e.,  $\mathbf{f}_0$ ,  $\mathbf{f}_l$ ,  $v_{l,k}$  and  $q_k$ , are modeled as Rayleigh fading and given as  $\mathbf{a} = \zeta_a^{1/2} \tilde{\mathbf{a}}$ , where  $\mathbf{a} \in \{\mathbf{f}_0, \mathbf{f}_l, v_{l,k}, q_k\}$  and  $\zeta_a$  is the large-scale path-loss and shadowing, which stays constant for several coherence intervals. Moreover,  $\tilde{\mathbf{a}} \sim \mathcal{CN}(\mathbf{0}, \mathbf{I}_A)$  accounts for the small-scale Rayleigh fading, where  $A \in \{M, 1\}$ .

Conversely, following the echo signal representation in multiple-input and multiple-output (MIMO) radar systems, the channels between the BS and tags, i.e.,  $\mathbf{g}_{f,k}$  and  $\mathbf{g}_{b,k}$ , are modeled as line-of-sight (LoS) channels [13]. The transmit/receiver array steering vectors to the direction  $\theta_k$  are thus denoted as

$$\mathbf{b}(\theta_k) = \sqrt{\frac{\zeta_b}{B}} \left[ 1, e^{j\pi \sin(\theta_k)}, \dots, e^{j\pi(B-1) \sin(\theta_k)} \right]^T, \quad (1)$$

where  $\mathbf{b} \in \{\mathbf{g}_{f,k}, \mathbf{g}_{b,k}\}$ ,  $B \in \{M, N\}$ ,  $\theta_k$  is  $T_k$ 's direction for the BS and the reader direction, and  $\zeta_b$  denotes the path-loss. Finally,  $\mathbf{G}_{\text{SI}} \in \mathbb{C}^{M \times N}$  is the SI channel matrix between the transmitter and the receiver antennas of the BS and is modeled as a Rician fading channel with a Rician factor of  $K_{\text{SI}}$  [14], [26].

Channel state information (CSI) is essential for BS beamforming, user/reader data decoding, and other operations. To acquire CSI, the proposed system is assumed to utilize the time-division duplexing mode. That means coherence time is divided into two slots, one designated for channel estimation and one for data transmission. In the first slot, pilot signals are transmitted, which can yield high-quality CSI. Passive tags, however, have restricted pilot transmission capabilities [27]. Instead, they can modulate pilot sequences into the BS signal and reflect them to the reader, allowing the channel estimation via least square (LS)/MMSE estimate and deep learning [28], [29]. Although not the focus of this study, backscatter CSI estimation is complex, and recent results [29] are promising. Thus, full CSI availability is a reasonable assumption.

### C. Transmission Model

The BS serves the primary users and simultaneously receives the tag-reflected signals. The BS applies RSMA to send messages to the primary users. In particular, the message  $d_l$  of  $U_l$  is split into a common part  $d_{c,l}$  and a private part  $d_{p,l}$ , i.e.,  $d_l = \{d_{c,l}, d_{p,l}\}$  for  $l \in \mathcal{L}$ . The common parts of all users, i.e.,  $\{d_{c,1}, \dots, d_{c,L}\}$  are jointly encoded into the common stream  $x_c$  while the private parts, i.e.,  $\{d_{p,1}, \dots, d_{p,L}\}$  are respectively encoded into private streams  $\{x_1, \dots, x_L\}$ , which are assumed to be independent [15]. The common stream and the private streams are then linearly precoded before transmission using the precoders  $\mathbf{w}_c \in \mathbb{C}^{M \times 1}$  and  $\mathbf{w}_l \in \mathbb{C}^{M \times 1}$  for  $l \in \mathcal{L}$ , respectively.

Conversely, the BS signal also includes sensing signal  $\mathbf{s} \in \mathbb{C}^{M \times 1}$  with the covariance matrix  $\mathbf{S} \triangleq \mathbb{E}\{\mathbf{s}\mathbf{s}^H\}$ . This extends the degrees-of-freedom of the transmitted signal  $\mathbf{x}$  to achieve enhanced sensing performance [13]. The BS transmitted signal can be expressed as

$$\mathbf{x} = \mathbf{w}_c x_c + \sum_{j \in \mathcal{L}} \mathbf{w}_j x_j + \mathbf{s}. \quad (2)$$

In (2), it is assumed that  $x_c$ ,  $\{x_l\}_{l \in \mathcal{L}}$ , and  $\mathbf{s}$  are independent of each other.

To backscatter data, tag  $T_k$  uses a multi-level ( $\tilde{M}$ -ary) modulation scheme [3], [4]. Tag data symbol  $c_k$ , with  $\mathbb{E}\{|c_k|^2\} = 1$ , is thus selected from a  $\tilde{M}$ -ary constant-envelope modulation. Consequently, the users receive the BS signal and the tags' backscattered signals. Assuming the propagation delay difference for all signals is negligible [30], the received signal at  $U_l$  is given by

$$y'_l = \mathbf{f}_l^H \mathbf{x} + \sum_{k \in \mathcal{K}} \sqrt{\alpha_k} \mathbf{h}_{l,k}^H \mathbf{x} c_k + z_u, \quad (3)$$

where the first and second terms are the direct-link signals (BS-to-user) and the backscatter-link signals (BS-to-tags-to-user), respectively,  $z_u \sim \mathcal{CN}(0, \sigma^2)$  is the additive white Gaussian noise (AWGN) at  $U_l$ , with 0 mean and  $\sigma^2$  variance, and  $\mathbf{h}_{l,k}$  is the effective backscatter channel at  $U_l$  through  $T_k$ , i.e.,  $\mathbf{h}_{l,k} = \mathbf{g}_{f,k}(\theta_k) v_{l,k}$ . Because primary users and BS are integral to the primary networks, a pre-existing connection permits the exchange of information, including sensing waveforms, via a control link [25]. It is thus assumed that the users are aware of the sensing waveform, however, partially eliminate it before decoding data. This is due to the limited dynamic range of the users, even if the channels are perfectly known. After the detecting signal is removed, the received signal is given as

$$y_l = \mathbf{f}_l^H \mathbf{w}_c x_c + \sum_{j \in \mathcal{L}} \mathbf{f}_l^H \mathbf{w}_j x_j + \sqrt{\delta_s} \mathbf{f}_l^H \mathbf{s} + \sum_{k \in \mathcal{K}} \sqrt{\alpha_k} \mathbf{h}_{l,k}^H \left( \mathbf{w}_c x_c + \sum_{j \in \mathcal{L}} \mathbf{w}_j x_j + \mathbf{s} \right) c_k + z_u, \quad (4)$$

where  $\delta_s \in [0, 1]$  accounts for the SIC quality for the sensing signal.

As the reader and the BS cooperate, the reader is aware of the BS transmitted signal. The reader thus applies SIC before decoding tags data. The post-processed received signal at the reader is given as

$$y_r = \sqrt{\delta_c} \mathbf{f}_0^H \mathbf{w}_c x_c + \sqrt{\delta_p} \sum_{j \in \mathcal{L}} \mathbf{f}_0^H \mathbf{w}_j x_j + \sqrt{\delta_s} \mathbf{f}_0^H \mathbf{s}$$

$$+ \sum_{k \in \mathcal{K}} \sqrt{\alpha_k} \mathbf{h}_k^H \left( \mathbf{w}_c x_c + \sum_{j \in \mathcal{L}} \mathbf{w}_j x_j + \mathbf{s} \right) c_k + z_r, \quad (5)$$

where  $\mathbf{h}_k = \mathbf{g}_{f,k}(\theta_k) q_k$  and  $z_r \sim \mathcal{CN}(0, \sigma^2)$  is the AWGN at the reader. Moreover,  $\delta_c \in [0, 1]$  and  $\delta_p \in [0, 1]$  are the SIC qualities for the common stream and private streams, respectively.

Tag backscattered signals reach the users, reader, and BS. Thus, those signals enable the BS to retrieve environmental information [6]. The BS received signal, i.e.,  $\mathbf{y}_b \in \mathbb{C}^{N \times 1}$ , is given as

$$\mathbf{y}_b = \sum_{k \in \mathcal{K}} \sqrt{\alpha_k} \mathbf{G}_k(\theta_k) \mathbf{x} c_k + \mathbf{G}_{\text{SI}}^H \mathbf{x} + \mathbf{z}_b, \quad (6)$$

where  $\mathbf{G}_k(\theta_k) \triangleq \mathbf{g}_{b,k}(\theta_k) \mathbf{g}_{f,k}^H(\theta_k)$ ,  $\sqrt{\alpha_k} \mathbf{G}_k(\theta_k) \mathbf{x} c_k$  is  $T_k$ 's ( $k$ -th target) reflection, and  $\mathbf{z}_b \sim \mathcal{CN}(\mathbf{0}, \sigma^2 \mathbf{I}_N)$  is the AWGN at the BS. In (6), the second term is the SI at the BS receiver due to simultaneous transmission and reception. Due to the limited dynamic range of the receiver, SI cannot be canceled perfectly even with the perfect CSI of the SI channel [14]. After the SI cancellation, the BS applies the receiver beamformer,  $\mathbf{u}_k \in \mathbb{C}^{N \times 1}$  for  $k \in \mathcal{K}$ , to the received signal (6) to acquire the desired reflected signal of  $T_k$ . The post-processed signal for acquiring  $T_k$  sensing information is thus given as

$$y_{b,k} = \sqrt{\alpha_k} \mathbf{u}_k^H \mathbf{G}_k(\theta_k) \mathbf{x} c_k + \sum_{i \in \mathcal{K}_k} \sqrt{\alpha_i} \mathbf{u}_k^H \mathbf{G}_i(\theta_i) \mathbf{x} c_i + \sqrt{\beta} \mathbf{u}_k^H \mathbf{G}_{\text{SI}}^H \mathbf{x} + \mathbf{u}_k^H \mathbf{z}_b, \quad (7)$$

where  $\mathcal{K}_k \triangleq \mathcal{K} \setminus \{k\}$  and  $0 < \beta \ll 1$  is a constant denoting the SI cancellation ability of the FD BS, i.e., the SI cancellation quality. FD radios can use SI cancellation techniques involving hardware techniques, analog domain cancellation, and digital domain cancellation of residual SI [14]. These can also be adapted for ISAC/ISABC systems.

### D. Tags' EH

As mentioned, passive tags do not generate RF signals and rely entirely on EH to power their essential functions. To simultaneously perform EH and data transfer operations, tags split the incident RF signal [31], [32] into two streams. With this PS,  $T_k$  reflects a fraction of the incident RF power, i.e.,  $p_k^{\text{in}} = |\mathbf{g}_{f,k}^H \mathbf{w}|^2 + \mathbf{g}_{f,k}^H \mathbf{S} \mathbf{g}_{f,k}$ , and harvests the remainder based on the reflection coefficient,  $\alpha_k$  [31]. In particular,  $T_k$  reflects  $\alpha_k p_k^{\text{in}}$  or data transmission, while absorbing the remainder,  $(1 - \alpha_k) p_k^{\text{in}}$ , for EH.

The harvested power at  $T_k$ ,  $p_k^{\text{h}}$ , can be modeled as a linear or nonlinear function of  $p_k^{\text{in}}$ . The harvested power of the widely used linear model is given as  $p_k^{\text{h}} = \eta(1 - \alpha_k) p_k^{\text{in}}$ , where  $\eta \in (0, 1]$  is the power conversion efficiency. Despite its simplicity, the linear EH model overlooks nonlinear characteristics of actual EH circuits, such as saturation and sensitivity [33]. As a remedy, a parametric nonlinear EH model based on the sigmoid function has been frequently employed [33]. It models the total harvested power at  $T_k$  as  $p_k^{\text{h}} = \Phi((1 - \alpha_k) p_k^{\text{in}})$ , where  $\Phi(\cdot)$  is a function representing non-linear effects [33, eq. (4)].

Nevertheless, our problem formulation can handle linear and non-linear models within one unified framework. The activation threshold,  $p_b$ , is an essential parameter whether a

linear or non-linear model is used. It is the minimal amount of power necessary to activate the EH circuit, which is around  $-20$  dBm for off-the-shelf passive tags [3]. This means that the harvested power must exceed  $p_b$  to activate the tag, i.e.,  $(1 - \alpha_k)p_k^{\text{in}} \geq p'_b$ , where  $p'_b \triangleq \Phi^{-1}(p_b)$ . The following utilizes the nonlinear EH model to formulate the optimization problem and design the resource allocation algorithm.

### III. COMMUNICATION AND SENSING PERFORMANCE

This section derives the communication and sensing performance of the proposed RSMA-assisted ISABC system.

#### A. Primary Communication Performance

The users first decode the common message by treating private and backscatter signals as interference. From (4), the rate of  $U_l$  for decoding common data is

$$\mathcal{R}_{c,l} = \log_2(1 + \gamma_{c,l}), \quad (8)$$

where  $\gamma_{c,l}$  is the received SINR at  $U_l$  for decoding  $x_c$ , and given in (9). To guarantee that all users successfully decode the common stream, the rate of decoding the common stream  $x_c$  should not exceed  $\mathcal{R}_c = \min_{l \in \mathcal{L}} \mathcal{R}_{c,l}$  [17]. As  $\mathcal{R}_c$  is shared by  $L$  users, it follows that  $\sum_{l \in \mathcal{L}} C_l = \mathcal{R}_c$ , where  $C_l$  is the portion of the common rate at  $U_l$  transmitting  $d_{c,l}$ .

Next,  $U_l$  subtracts the decoded common message from the received signal and decodes its desired private message,  $x_l$ . The private rate of  $U_l$  is thus given by

$$\mathcal{R}'_{p,l} = \log_2(1 + \gamma_{p,l}), \quad (10)$$

where  $\gamma_{p,l}$  is the received SINR at  $U_l$  for decoding  $x_l$  and given in (11). In (11)  $\delta_c$  accounts for SIC qualities for removing the common signal. The total achievable rate of  $U_l$ , including the portion of common rate transmitting  $d_{c,l}$  and private rate transmitting  $d_{p,l}$ , is thus expressed as

$$\mathcal{R}_{p,l} = C_l + \mathcal{R}'_{p,l}. \quad (12)$$

#### B. BackCom Performance

The reader decodes the tags' data. Using (5), the reader decodes  $T_k$ 's data at the rate

$$\mathcal{R}_{t,k} \approx \log_2(1 + \gamma_{t,k}), \quad (13)$$

where  $\gamma_{t,k}$  is the  $T_k$ 's SINR at the reader and given in (14).

#### C. Sensing Performance

Sensing performance is typically measured by the transmit beam pattern gain or mean squared error of the transmit beam pattern [34], [35]. Although simple, they do not account for the receiver's beam pattern or multi-target interference. This may cause ambiguity in multi-target detection due to interference between the targets' reflected signals [13], [36]. To overcome the limitations in such sensing measures, the sensing SINR has been suggested to assess sensing performance [13], [36]. The detection probability of a target (tag) is proportional to its sensing SINR [13], [36]. In addition, the sensing SINR enables target detection through both transmit and receiver

beamforming, reducing interference between targets [13], [36]. Due to these benefits, this study employs sensing SINR to measure sensing performance.

Sensing is done by the BS, which utilizes the backscattered signal of tag  $T_k$ . The BS applies the SI cancellation and the receiver beamformer,  $\mathbf{u}_k$ , to received signal (6) to capture  $T_k$ 's reflected signal. From (7), the sensing rate of  $T_k$  is obtained as

$$\mathcal{R}_{s,k} \approx \log_2(1 + \Upsilon_k), \quad (15)$$

where  $\Upsilon_k$  is the sensing SINR of  $T_k$  and given in (16).  $\mathbf{R}_x \triangleq \mathbb{E}\{\mathbf{x}\mathbf{x}^H\} = \mathbf{w}_c\mathbf{w}_c^H + \sum_{j \in \mathcal{L}} \mathbf{w}_j\mathbf{w}_j^H + \mathbf{S}$  in (16) is the BS transmitted signal covariance matrix [13].

### IV. PROBLEM FORMULATION

Herein, the BS transmit power of the proposed RSMA-assisted ISABC network is optimized. In particular, our objective is to minimize it by jointly optimizing the BS receive beamforming,  $\{\mathbf{u}_k\}_{k \in \mathcal{K}}$ , the BS transmit beamforming,  $\mathbf{w}_c$ ,  $\{\mathbf{w}_l\}_{l \in \mathcal{L}}$ , covariance matrix  $\mathbf{S}$ , the tag reflection coefficients,  $\{\alpha_k\}_{k \in \mathcal{K}}$ , and common rates of the users,  $\{C_l\}_{l \in \mathcal{L}}$ . The set of all the optimization variables is denoted as  $\mathcal{A} = \{\{\mathbf{u}_k\}_{k \in \mathcal{K}}, \mathbf{w}_c, \{\mathbf{w}_l\}_{l \in \mathcal{L}}, \mathbf{S} \succeq 0, \{\alpha_k\}_{k \in \mathcal{K}}, \{C_l\}_{l \in \mathcal{L}}\}$ .

The communication rates for the users and the reader must exceed their thresholds. The sensing and EH functionalities of the tags must be met. The optimization problem is thus formulated as follows:

$$\mathbf{P}_1 : \min_{\mathcal{A}} \quad \|\mathbf{w}_c\|^2 + \sum_{l \in \mathcal{L}} \|\mathbf{w}_l\|^2 + \text{Tr}(\mathbf{S}), \quad (17a)$$

$$\text{s.t.} \quad \mathcal{R}_{s,k} \geq \mathcal{R}_{s,k}^{\text{th}}, \quad \forall k, \quad (17b)$$

$$\mathcal{R}_{t,k} \geq \mathcal{R}_{t,k}^{\text{th}}, \quad \forall k, \quad (17c)$$

$$\mathcal{R}_{c,l} \geq \mathcal{R}_{c,l}^{\text{th}}, \quad \forall l, \quad (17d)$$

$$C_l + \mathcal{R}'_{p,l} \geq \mathcal{R}_{p,l}^{\text{th}}, \quad \forall l, \quad (17e)$$

$$\sum_{l \in \mathcal{L}} C_l \leq \mathcal{R}_c, \quad (17f)$$

$$0 \leq C_l \leq \mathcal{R}_{p,l}^{\text{th}}, \quad \forall l, \quad (17g)$$

$$p_k^{\text{in}} \geq \frac{\Phi^{-1}(p_b)}{1 - \alpha_k}, \quad \forall k, \quad (17h)$$

$$\mathbf{S} \succeq 0, \quad (17i)$$

$$\|\mathbf{u}_k\|^2 = 1, \quad \forall k, \quad (17j)$$

$$0 < \alpha_k < 1, \quad \forall k, \quad (17k)$$

where constraints (17b) and (17c) ensure the required sensing and communication rate requirement of each tag at the BS and the reader, respectively, with  $\mathcal{R}_{s,k}^{\text{th}}$  and  $\mathcal{R}_{t,k}^{\text{th}}$  representing the corresponding targeted sensing and BackCom rates. On the other hand, (17d) and (17e) set the minimum rate requirements for the user to decode common and private data, respectively, in which  $\mathcal{R}_{c,l}^{\text{th}}$  and  $\mathcal{R}_{p,l}^{\text{th}}$  denote the targeted common and private rates of respective user. Conditions (17f) and (17g) are necessary to guarantee the successful decoding of the common stream. Besides, (17h) guarantees the minimum tag power requirements for EH. Constraint (17j) is the normalization constraint for the BS reception filter. Finally, (17k) is the range of the tag reflection coefficient.

$$\gamma_{c,l} = \frac{|\mathbf{f}_l^H \mathbf{w}_c|^2}{\sum_{j \in \mathcal{L}} |\mathbf{f}_l^H \mathbf{w}_j|^2 + \delta_s |\mathbf{f}_l^H \mathbf{s}|^2 + \sum_{k \in \mathcal{K}} \alpha_k \left( |\mathbf{h}_{l,k}^H \mathbf{w}_c|^2 + \sum_{j \in \mathcal{L}} |\mathbf{h}_{l,k}^H \mathbf{w}_j|^2 + |\mathbf{h}_{l,k}^H \mathbf{s}|^2 \right) + \sigma^2} \quad (9)$$

$$\gamma_{p,l} = \frac{|\mathbf{f}_l^H \mathbf{w}_l|^2}{\delta_c |\mathbf{f}_l^H \mathbf{w}_c|^2 + \sum_{j \in \mathcal{L}_l} |\mathbf{f}_l^H \mathbf{w}_j|^2 + \delta_s |\mathbf{f}_l^H \mathbf{s}|^2 + \sum_{k \in \mathcal{K}} \alpha_k \left( |\mathbf{h}_{l,k}^H \mathbf{w}_c|^2 + \sum_{j \in \mathcal{L}} |\mathbf{h}_{l,k}^H \mathbf{w}_j|^2 + |\mathbf{h}_{l,k}^H \mathbf{s}|^2 \right) + \sigma^2} \quad (11)$$

$$\gamma_{t,k} = \frac{\alpha_k \left( |\mathbf{h}_k^H \mathbf{w}_c|^2 + \sum_{j \in \mathcal{L}} |\mathbf{h}_k^H \mathbf{w}_j|^2 + |\mathbf{h}_k^H \mathbf{s}|^2 \right)}{\delta_c |\mathbf{f}_0 \mathbf{w}_c|^2 + \delta_p \sum_{j \in \mathcal{L}} |\mathbf{f}_0^H \mathbf{w}_j|^2 + \delta_s |\mathbf{f}_0^H \mathbf{s}|^2 + \sum_{i \in \mathcal{K}_k} \alpha_i \left( |\mathbf{h}_i^H \mathbf{w}_c|^2 + \sum_{j \in \mathcal{L}} |\mathbf{h}_i^H \mathbf{w}_j|^2 + |\mathbf{h}_i^H \mathbf{s}|^2 \right) + \sigma^2} \quad (14)$$

$$\Upsilon_k = \frac{\alpha_k \mathbb{E} \{ |\mathbf{u}_k^H \mathbf{G}_k(\theta_k) \mathbf{x}|^2 \}}{\sum_{i \in \mathcal{K}_k} \alpha_i \mathbb{E} \{ |\mathbf{u}_k^H \mathbf{G}_i(\theta_i) \mathbf{x}|^2 \} + \beta \mathbb{E} \{ |\mathbf{u}_k^H \mathbf{G}_{\text{SI}}^H \mathbf{x}|^2 \} + \mathbb{E} \{ |\mathbf{u}_k^H \mathbf{z}_b|^2 \}} = \frac{\alpha_k \mathbf{u}_k^H \mathbf{G}_k(\theta_k) \mathbf{R}_x \mathbf{G}_k^H(\theta_k) \mathbf{u}_k}{\mathbf{u}_k^H \left( \sum_{i \in \mathcal{K}_k} \alpha_i \mathbf{G}_i(\theta_i) \mathbf{R}_x \mathbf{G}_i^H + \beta \mathbf{G}_{\text{SI}} \mathbf{R}_x \mathbf{G}_{\text{SI}}^H + \sigma^2 \mathbf{I}_N \right) \mathbf{u}_k} \quad (16)$$

Since the user/tag communication/sensing rates are monotonically increasing functions of their arguments, i.e., SINRs, they can be replaced with respective SINRs before proceeding to the proposed solution. The optimization problem,  $\mathbf{P}_1$ , is thus equivalently formulated as follows:

$$\mathbf{P}_2 : \min_{\mathcal{A}} \quad \|\mathbf{w}_c\|^2 + \sum_{l \in \mathcal{L}} \|\mathbf{w}_l\|^2 + \text{Tr}(\mathbf{S}), \quad (18a)$$

$$\text{s.t.} \quad \Upsilon_k \geq \Upsilon_k^{\text{th}}, \quad \forall k, \quad (18b)$$

$$\gamma_{t,k} \geq \Gamma_{t,k}^{\text{th}}, \quad \forall k, \quad (18c)$$

$$\gamma_{c,l} \geq \Gamma_{c,l}^{\text{th}}, \quad \forall l, \quad (18d)$$

$$(17e) - (17k), \quad (18e)$$

where  $\Upsilon_k^{\text{th}} \triangleq 2^{\mathcal{R}_{s,k}^{\text{th}}} - 1$ ,  $\Gamma_{t,k}^{\text{th}} \triangleq 2^{\mathcal{R}_{t,k}^{\text{th}}} - 1$ , and  $\Gamma_{c,l}^{\text{th}} \triangleq 2^{\mathcal{R}_{c,l}^{\text{th}}} - 1$  are the respective sensing/communication SINR thresholds.

## V. PROPOSED SOLUTION

Since problem  $\mathbf{P}_2$  is non-convex, widely available convex algorithms cannot be directly applied. Thus, an AO strategy [20] is adopted to handle it, where the problem is decomposed into three sub-problems [37]. It turns out that the objective value of  $\mathbf{P}_2$  is the same regardless of the solutions of the first and third sub-problems. Thus, they are feasibility problems. Feasibility problems aim to find any solution that satisfies the constraints. However, these are converted into optimization problems with explicit objectives for more effective solutions.

### A. Sub-Problem 1: Optimizing over $\mathbf{u}_k$

This develops the optimal reception filters of the BS while keeping other variables constant. For given  $\{\mathbf{w}_c, \{\mathbf{w}_l\}_{l \in \mathcal{L}}, \mathbf{S}, \{\alpha_k\}_{k \in \mathcal{K}}, \{C_l\}_{l \in \mathcal{L}}\}$ ,  $\mathbf{P}_2$  becomes a feasibility problem. Therefore, any feasible value of  $\mathbf{u}_k$  that complies with (18b) and (17j) can be a potential solution.

Although vector  $\mathbf{u}_k$  may not have a direct impact on reducing the BS transmit power, it is crucial for optimizing the sensing SINR at the BS for each tag. Our methodology prioritizes the optimization of  $\mathbf{u}_k$  to meet the sensing performance criteria and indirectly contribute to transmit power

reduction. Enhanced SINR for tag signals reduces the need for higher transmit power, thus aligning with our overarching aim of power minimization [38], [39].

Using the unique structure of the sensing SINR for each tag (16), this sub-problem is transformed into a generalized Rayleigh quotient problem, providing closed-form optimal combiner vectors [38]. To this end,  $\mathbf{P}_2$  is reduced to the following optimization problem:

$$\mathbf{P}_u : \max_{\mathbf{u}_k} \frac{\alpha_k \mathbf{u}_k^H \mathbf{G}_k \mathbf{R}_x \mathbf{G}_k^H \mathbf{u}_k}{\mathbf{u}_k^H \left( \sum_{i \in \mathcal{K}_k} \alpha_i \mathbf{G}_i \mathbf{R}_x \mathbf{G}_i^H + \beta \mathbf{G}_{\text{SI}} \mathbf{R}_x \mathbf{G}_{\text{SI}}^H + \sigma_k^2 \mathbf{I}_N \right) \mathbf{u}_k}, \quad (19a)$$

$$\text{s.t.} \quad \|\mathbf{u}_k\|^2 = 1, \quad \forall k, \quad (19b)$$

Next, the objective function, (19a), is rearranged to convert it into the following optimization problem:

$$\mathbf{P}_{u1} : \max_{\mathbf{u}_k} \frac{\mathbf{u}_k^H \tilde{\mathbf{G}}_k \tilde{\mathbf{G}}_k^H \mathbf{u}_k}{\mathbf{u}_k^H \mathbf{Q}_k \mathbf{u}_k}, \quad (20a)$$

$$\text{s.t.} \quad (19b), \quad (20b)$$

where  $\mathbf{Q}_k \triangleq \sum_{i \in \mathcal{K}_k} \alpha_i \mathbf{G}_i \mathbf{R}_x \mathbf{G}_i^H + \beta \mathbf{G}_{\text{SI}} \mathbf{R}_x \mathbf{G}_{\text{SI}}^H + \sigma^2 \mathbf{I}_N$ , and  $\tilde{\mathbf{G}}_k = \sqrt{\alpha_k} \mathbf{G}_k (\mathbf{w}_c + \sum_{j \in \mathcal{L}} \mathbf{w}_j + \mathbf{s})$ . Problem  $\mathbf{P}_{u1}$  thus becomes a generalized Rayleigh ratio quotient problem [38]. The optimal combiner vector for  $T_k$  is characterized by the Wiener or MMSE filter [32] and is given as

$$\mathbf{u}_k^* = \frac{\mathbf{Q}_k^{-1} \tilde{\mathbf{G}}_k}{\|\mathbf{Q}_k^{-1} \tilde{\mathbf{G}}_k\|}, \quad \forall k. \quad (21)$$

### B. Sub-Problem 2: Optimizing over $\mathbf{w}_c$ , $\mathbf{w}_l$ , $\mathbf{S}$ , and $C_l$

This optimizes for the BS transmit beamforming, i.e.,  $\mathbf{w}_c$ ,  $\{\mathbf{w}_l\}_{l \in \mathcal{L}}$ , and  $\mathbf{S}$ , and users' common rate, i.e.,  $\{C_l\}_{l \in \mathcal{L}}$  for given  $\{\{\mathbf{u}_k\}_{k \in \mathcal{K}}, \{\alpha\}_{k \in \mathcal{K}}\}$ . However, owing to the interference within the SINRs, Constraints  $\mathbf{P}_2$  become non-convex for the BS transmit beamformers. The semi-definite relaxation

(SDR) method is employed to overcome this barrier. Thus,  $\mathbf{P}_2$  is reformulated as

$$\mathbf{P}_w : \min_{\mathbf{w}_c, \mathbf{w}_l, \mathbf{S}, C_l} \|\mathbf{w}_c\|^2 + \sum_{l \in \mathcal{L}} \|\mathbf{w}_l\|^2 + \text{Tr}(\mathbf{S}), (22a)$$

s.t. (18b) – (18d), (17e) – (17i). (22b)

$\mathbf{P}_w$  can be effectively addressed by using the SDR method [21], [22]. Define matrices  $\mathbf{W}_c \triangleq \mathbf{w}_c \mathbf{w}_c^H$  and  $\mathbf{W}_l \triangleq \mathbf{w}_l \mathbf{w}_l^H$  for  $l \in \mathcal{L}$ . Here,  $\mathbf{W}_c$  and  $\mathbf{W}_l$  are semi-definite matrices with rank one constraints, i.e.,  $\text{Rank}(\mathbf{W}_c) = 1$  and  $\text{Rank}(\mathbf{W}_l) = 1$ . By relaxing the highly non-convex rank one constraints,  $\mathbf{P}_w$  can be reformulated into a conventional semi-definite programming (SDP) problem. However, as constraints (17e) and (17f) are still non-convex, they are next converted into tractable convex forms. Define

$$A_l \triangleq \text{Tr}(\mathbf{f}_l \mathbf{f}_l^H \mathbf{W}_l), (23a)$$

$$B_l \triangleq \delta_c \text{Tr}(\mathbf{f}_l \mathbf{f}_l^H \mathbf{W}_c) + \sum_{j \in \mathcal{L}_l} |\text{Tr}(\mathbf{f}_l \mathbf{f}_l^H \mathbf{W}_j)| + \delta_s \text{Tr}(\mathbf{f}_l \mathbf{f}_l^H \mathbf{S})$$

$$+ \sum_{k \in \mathcal{K}} \alpha_k \left( \text{Tr}(\mathbf{h}_{l,k} \mathbf{h}_{l,k}^H \mathbf{W}_c) + \sum_{j \in \mathcal{L}} \text{Tr}(\mathbf{h}_{l,k} \mathbf{h}_{l,k}^H \mathbf{W}_j) + \text{Tr}(\mathbf{h}_{l,k} \mathbf{h}_{l,k}^H \mathbf{S}) \right) + \sigma^2. (23b)$$

The SINR in (17e) is now bounded such that  $0 \leq \mu_l \leq A_l/B_l$ , where  $\mu_l$  is an auxiliary variable. Thereby introducing another auxiliary variable,  $\phi_l$ , where  $A_l \geq \mu_l \phi_l$  and  $B_l \leq \phi_l$ . However, since the product  $\mu_l \phi_l$  is non-convex, Taylor-series linearization is used to convert it to a convex function as

$$\mu_l \phi_l = \mu_l^{(t)} \phi_l^{(t)} + \phi_l^{(t)} (\mu_l - \mu_l^{(t)}) + \mu_l^{(t)} (\phi_l - \phi_l^{(t)}) \triangleq v_l, (24)$$

where  $\{\mu_l, \phi_l\}$  and  $\{\mu_l^{(t)}, \phi_l^{(t)}\}$  are the current and the previous iteration values of  $\{\mu_l, \phi_l\}$ , respectively. The constraint (17e) is thus equivalent to

$$\begin{cases} C_l + \log_2(1 + \mu_l) \geq \mathcal{R}_{p,l}^{\text{th}}, & \forall l, & (25a) \\ A_l \geq v_l, & \forall l, & (25b) \\ B_l \leq \phi_l, & \forall l. & (25c) \end{cases}$$

For constraint (17f), each rate value  $\mathcal{R}_c$  is replaced with  $\sum_{l \in \mathcal{L}} C_l \leq \mathcal{R}_c$ ,  $l$  for  $l \in \mathcal{L}$ . Since  $\mathcal{R}_c$ ,  $l$  is not a convex function of the optimization variables, the successive convex approximation (SCA) method is employed to linearize the constraint as

$$\sum_{l \in \mathcal{L}} C_l \leq F_l - \tilde{F}_l, (26)$$

where  $F_l$  and  $\tilde{F}_l$  are given in (27) and (28), respectively, and  $\Lambda_l$  is defined as

$$\Lambda_l \triangleq \sum_{j \in \mathcal{L}} \text{Tr}(\mathbf{f}_l \mathbf{f}_l^H \mathbf{W}_j^{(t)}) + \delta_s \text{Tr}(\mathbf{f}_l \mathbf{f}_l^H \mathbf{S}^{(t)})$$

$$+ \sum_{k \in \mathcal{K}} \alpha_k \left( \text{Tr}(\mathbf{h}_{l,k} \mathbf{h}_{l,k}^H \mathbf{W}_c^{(t)}) + \sum_{j \in \mathcal{L}} \text{Tr}(\mathbf{h}_{l,k} \mathbf{h}_{l,k}^H \mathbf{W}_j^{(t)}) + \text{Tr}(\mathbf{h}_{l,k} \mathbf{h}_{l,k}^H \mathbf{S}^{(t)}) \right) + \sigma^2. (29)$$

In (29),  $(\cdot)^{(t)}$  denotes the previous iteration values of respective variables. Finally,  $\mathbf{P}_w$  can be reformulated to a relaxed

SDP problem as given in (30), which can be tackled using the CVX tool [40], [41].

If the solutions to the relaxed problem  $\mathbf{P}_{w1}$  are of rank one, the optimal transmit beamformers are obtained by eigenvalue decomposition [22]. Let the eigenvalue decomposition of  $\mathbf{W}$  (i.e.,  $\mathbf{W} \in \{\mathbf{W}_c^*, \{\mathbf{W}_l^*\}_{l \in \mathcal{L}}\}$ ) to be  $\mathbf{W} = \mathbf{U} \mathbf{\Sigma} \mathbf{U}^H$ , where  $\mathbf{U}$  is a unitary matrix and  $\mathbf{\Sigma} = \text{diag}(\lambda_1, \dots, \lambda_M)$  is a diagonal matrix. If  $\mathbf{W}^*$  is rank one, the optimal transmit beamformer,  $\mathbf{w}^*$ , is the eigenvector for the maximum eigenvalue. If not, the Gaussian randomization accounts for the relaxed rank-one constraint [22]. Specifically, a solution for  $\mathbf{P}_w$  is generated as  $\tilde{\mathbf{W}} = \mathbf{U} \mathbf{\Sigma}^{1/2} \mathbf{r}$ , with  $\mathbf{r} \in \mathcal{CN}(0, \mathbf{I}_M)$ . Such solutions are tested for  $10^5$  times, and the best one is selected. These numerous random realizations of  $\mathbf{r}$  with the SDR technique ensure an  $\frac{\pi}{4}$ -approximation to the optimal value of  $\mathbf{P}_w$  [21], [22].

### C. Sub-Problem 3: Optimizing over $\alpha_k$

This final sub-problem requires optimizing  $\{\alpha_k\}_{k \in \mathcal{K}}$  for given  $\{\mathbf{w}_c, \{\mathbf{w}_l\}_{l \in \mathcal{L}}, \mathbf{S}, \{\mathbf{u}_k\}_{k \in \mathcal{K}}, \{C_l\}_{l \in \mathcal{L}}\}$ . Note that objective (18a) is not a function of the reflection coefficients of the tags. Thus, Sub-Problem 3 reduces to a constraint-satisfaction problem of  $\mathbf{P}_2$ . That is, any  $\{\alpha_k\}_{k \in \mathcal{K}}$  that satisfies the constraints (18b)–(18e) is considered to be an optimal solution. However, to effectively handle Sub-Problem 3, a slack-optimization-based problem is proposed [23]. While satisfying the other constraints, two new slack variables are introduced to optimize further the tags' SINR and EH margins, i.e.,  $t_1$  and  $t_2$ , respectively [23]. The proposed problem is thus given in (31), where  $\tilde{\Gamma}_{p,l}^{\text{th}} \triangleq \max(\Gamma_{c,l}^{\text{th}}, 2^{\sum_{l \in \mathcal{L}} C_l} - 1)$  and  $\tilde{\Gamma}_{p,l}^{\text{th}} \triangleq 2^{\mathcal{R}_{p,l}^{\text{th}} - C_l} - 1$ . In (31a),  $\lambda_1$  and  $\lambda_2$  are positive constants.  $\mathbf{P}_\alpha$  is convex, and thus can be efficiently solved by solvers such as CVX [41]. Introducing slack variables in  $\mathbf{P}_\alpha$  converts strict constraints into adjustable ones with a definable margin. This facilitates the convergence process by setting a more tangible minimization goal and aligns well with the convergence strategies of iterative solvers like CVX due to the explicit objective guiding the solution path [22], [23].

Algorithm 1 presents the overall steps to solve problem  $\mathbf{P}_1$  (17). It begins by setting  $\{\{\alpha_k\}_{k \in \mathcal{K}}, \mathbf{w}_c, \mathbf{w}_l, \mathbf{S}, C_l\}$  to random feasible values that satisfy the constraints in  $\mathbf{P}_1$ , and then refines the received/transmit beamforming, reflection coefficients, and common rate iteratively until the normalized reduction in the total transmit power is less than  $\epsilon = 10^{-3}$ .

Variable initialization assumes a crucial role in determining algorithm convergence. Closer initialization to optimal values typically accelerates convergence. However, complex optimization problems with numerous constraints pose challenges to finding a near-optimal starting guess, potentially escalating overall computing complexity [40]. Researchers often resort to randomly generating feasible initial values [22], [42], a strategy also embraced in this study. Nonetheless, simulation results show that our overall and individual algorithms achieve rapid convergence regardless of the random initial values.

**Remark 1.** *This study utilizes the AO method, and each associated subproblem yields a local solution. The convergence principle of the AO method is well-documented [20]. Simply*

$$F_l \triangleq \log_2 \left( \text{Tr}(\mathbf{f}_l \mathbf{f}_l^H \mathbf{W}_c) + \sum_{j \in \mathcal{L}} \text{Tr}(\mathbf{f}_l \mathbf{f}_l^H \mathbf{W}_j) + \delta_s \text{Tr}(\mathbf{f}_l \mathbf{f}_l^H \mathbf{S}) \right. \\ \left. + \sum_{k \in \mathcal{K}} \alpha_k \left( \text{Tr}(\mathbf{h}_{l,k} \mathbf{h}_{l,k}^H \mathbf{W}_c) + \sum_{j \in \mathcal{L}} \text{Tr}(\mathbf{h}_{l,k} \mathbf{h}_{l,k}^H \mathbf{W}_j) + \text{Tr}(\mathbf{h}_{l,k} \mathbf{h}_{l,k}^H \mathbf{S}) \right) + \sigma^2 \right) \quad (27)$$

$$\tilde{F}_l \triangleq \log_2(\Lambda_l) + \frac{\sum_{k \in \mathcal{K}} \alpha_k \text{Tr}(\mathbf{h}_{l,k} \mathbf{h}_{l,k}^H)}{\ln(2)\Lambda_l} \text{Tr}(\mathbf{W}_c - \mathbf{W}_c^{(t)}) + \sum_{j \in \mathcal{L}} \frac{\text{Tr}(\mathbf{f}_l \mathbf{f}_l^H) + \sum_{k \in \mathcal{K}} \alpha_k \text{Tr}(\mathbf{h}_{l,k} \mathbf{h}_{l,k}^H)}{\ln(2)\Lambda_l} \text{Tr}(\mathbf{W}_j - \mathbf{W}_j^{(t)}) \\ \frac{\delta_s \text{Tr}(\mathbf{f}_l \mathbf{f}_l^H) + \sum_{k \in \mathcal{K}} \alpha_k \text{Tr}(\mathbf{h}_{l,k} \mathbf{h}_{l,k}^H)}{\ln(2)\Lambda_l} \text{Tr}(\mathbf{S} - \mathbf{S}^{(t)}) \quad (28)$$

$$\mathbf{P}_{w1} : \min_{\mathbf{w}_c, \mathbf{w}_l, \mathbf{S}, C_l} \text{Tr}(\mathbf{W}_c) + \sum_{l \in \mathcal{L}} \text{Tr}(\mathbf{W}_l) + \text{Tr}(\mathbf{S}), \quad (30a)$$

$$\text{s.t. } \Upsilon_k^{\text{th}} \mathbf{u}_k^H \left( \sum_{i \in \mathcal{K}_k} \alpha_i \left( \text{Tr}(\mathbf{G}_i^H \mathbf{G}_i \mathbf{W}_c) + \sum_{j \in \mathcal{L}} \text{Tr}(\mathbf{G}_i^H \mathbf{G}_i \mathbf{W}_j) + \text{Tr}(\mathbf{G}_i^H \mathbf{G}_i \mathbf{S}) \right) + \sigma^2 \mathbf{I}_N \right. \\ \left. + \beta \left( \text{Tr}(\mathbf{G}_{\text{SI}}^H \mathbf{G}_{\text{SI}} \mathbf{W}_c) + \sum_{j \in \mathcal{L}} \text{Tr}(\mathbf{G}_{\text{SI}}^H \mathbf{G}_{\text{SI}} \mathbf{W}_j) + \text{Tr}(\mathbf{G}_{\text{SI}}^H \mathbf{G}_{\text{SI}} \mathbf{S}) \right) \right) \mathbf{u}_k \\ - \alpha_k \mathbf{u}_k^H \left( \text{Tr}(\mathbf{G}_k^H \mathbf{G}_k \mathbf{W}_c) + \sum_{j \in \mathcal{L}} \text{Tr}(\mathbf{G}_k^H \mathbf{G}_k \mathbf{W}_j) + \text{Tr}(\mathbf{G}_k^H \mathbf{G}_k \mathbf{S}) \right) \mathbf{u}_k \leq 0, \quad \forall k, \quad (30b)$$

$$\Gamma_{l,k}^{\text{th}} \left( \delta_c \text{Tr}(\mathbf{f}_0 \mathbf{f}_0^H \mathbf{W}_c) + \delta_p \sum_{j \in \mathcal{L}} \text{Tr}(\mathbf{f}_0 \mathbf{f}_0^H \mathbf{W}_j) + \delta_s \text{Tr}(\mathbf{f}_0 \mathbf{f}_0^H \mathbf{S}) + \sigma^2 + \sum_{i \in \mathcal{K}_k} \alpha_i \left( \text{Tr}(\mathbf{h}_i \mathbf{h}_i^H \mathbf{W}_c) + \sum_{j \in \mathcal{L}} \text{Tr}(\mathbf{h}_i \mathbf{h}_i^H \mathbf{W}_j) \right. \right. \\ \left. \left. + \text{Tr}(\mathbf{h}_i \mathbf{h}_i^H \mathbf{S}) \right) \right) - \alpha_k \left( \text{Tr}(\mathbf{h}_k \mathbf{h}_k^H \mathbf{W}_c) + \sum_{j \in \mathcal{L}} \text{Tr}(\mathbf{h}_k \mathbf{h}_k^H \mathbf{W}_j) + \text{Tr}(\mathbf{h}_k \mathbf{h}_k^H \mathbf{S}) \right) \leq 0, \quad \forall k, \quad (30c)$$

$$\Gamma_{c,l}^{\text{th}} \left( \sum_{j \in \mathcal{L}} \text{Tr}(\mathbf{f}_l \mathbf{f}_l^H \mathbf{W}_j) + \delta_s \text{Tr}(\mathbf{f}_l \mathbf{f}_l^H \mathbf{S}) + \sum_{i \in \mathcal{K}} \alpha_i \left( \text{Tr}(\mathbf{h}_{l,i} \mathbf{h}_{l,i}^H \mathbf{W}_c) + \sum_{j \in \mathcal{L}} \text{Tr}(\mathbf{h}_{l,i} \mathbf{h}_{l,i}^H \mathbf{W}_j) + \text{Tr}(\mathbf{h}_{l,i} \mathbf{h}_{l,i}^H \mathbf{S}) \right) + \sigma^2 \right) - \text{Tr}(\mathbf{f}_l \mathbf{f}_l^H \mathbf{W}_c) \leq 0, \quad \forall l, \quad (30d)$$

$$P_{\text{th}} - (1 - \alpha_k) \left( \text{Tr}(\mathbf{g}_{f,k} \mathbf{g}_{f,k}^H \mathbf{W}_c) + \sum_{j \in \mathcal{L}} \text{Tr}(\mathbf{g}_{f,k} \mathbf{g}_{f,k}^H \mathbf{W}_j) + \text{Tr}(\mathbf{g}_{f,k} \mathbf{g}_{f,k}^H \mathbf{S}) \right) \leq 0, \quad \forall k, \quad (30e)$$

$$\{\mathbf{W}_c, \{\mathbf{W}_l\}_{l \in \mathcal{L}}, \mathbf{S}\} \succeq 0, \quad (30f)$$

$$(17g), (25a) - (25c), (26). \quad (30g)$$

### Algorithm 1 Overall Algorithm

- 1: **Input:** Set the iteration counter  $t = 0$ , the convergence tolerance  $\epsilon > 0$ , initial feasible solution  $\{\{\alpha_k\}_{k \in \mathcal{K}}, \mathbf{w}_c, \mathbf{w}_l, \mathbf{S}, C_l\}$ . Initialize the objective function value  $F^{(0)} = 0$ .
- 2: **while**  $\frac{F^{(t+1)} - F^{(t)}}{F^{(t+1)}} \geq \epsilon$  **do**
- 3: Solve (21) to derive optimal received beamformer,  $\mathbf{u}_k^{(t+1)}$ .
- 4: Solve  $\mathbf{P}_{w1}$  (30) to obtain suboptimal transmit beamformers,  $\{\mathbf{w}_c^{(t+1)}, \mathbf{w}_l^{(t+1)}, \mathbf{S}^{(t+1)}, C_l^{(t+1)}\}$  by applying Gaussian randomization to recover the rank-one solution.
- 5: Solve  $\mathbf{P}_\alpha$  (31) to obtain the suboptimal power reflection coefficients,  $\alpha_k^{(t+1)}$ .
- 6: Calculate the objective function value  $F^{(t+1)}$ .
- 7: Set  $t \leftarrow t + 1$ ;
- 8: **end while**
- 9: **Output:** Optimal solutions  $\mathcal{A}^*$ .

put, if the individual sub-problems reach convergence, then the entire optimization process will converge as well [20]. This study employs the SDR and slack-optimization techniques to determine  $\{\mathbf{w}_c, \mathbf{w}_l, \mathbf{S}, C_l\}$  and  $\{\alpha_k\}_{k \in \mathcal{K}}$ , respectively. Meanwhile,  $\{\mathbf{u}_k\}_{k \in \mathcal{K}}$  is directly solved via the Rayleigh ratio quotient method. Both the SDR and slack-optimization are established methods with guaranteed convergence [22], reinforcing the convergence of our AO approach. Our simulation outcomes further validate this assertion (Fig. 2).

**Theorem 1.** Algorithm 1 iterations yield a non-increasing sequence of objective values with guaranteed convergence.

*Proof.* Please see Appendix A.  $\square$

### D. Complexity of Proposed Algorithm

The computational complexity of Algorithm 1 is analyzed.

1) *Optimization over  $\mathbf{u}_k$ :* Here, the Rayleigh quotient method provides the optimal closed-form received beamformers. It requires  $\mathcal{O}(N^3)$  complexity for computing the inverse of the matrix  $\mathbf{Q}$  while the MMSE filters for the  $K$  tags (21)



$$\mathbf{P}_\alpha : \quad \min_{\alpha_k, t_1, t_2} \lambda_1 t_1 + \lambda_2 t_2, \quad (31a)$$

$$\text{s.t.} \quad \alpha_k \mathbf{u}_k^H \mathbf{G}_k \mathbf{R}_x \mathbf{G}_k^H \mathbf{u}_k \geq \Upsilon_k^{\text{th}} \mathbf{u}_k^H \left( \sum_{i \in \mathcal{K}_k} \alpha_i \mathbf{G}_i \mathbf{R}_x \mathbf{G}_i^H + \beta \mathbf{G}_{\text{SI}} \mathbf{R}_x \mathbf{G}_{\text{SI}}^H + \sigma^2 \mathbf{I}_N \right) \mathbf{u}_k, \quad \forall k, \quad (31b)$$

$$\alpha_k \left( |\mathbf{h}_k^H \mathbf{w}_c|^2 + \sum_{j \in \mathcal{L}} |\mathbf{h}_k^H \mathbf{w}_j|^2 + \mathbf{h}_k^H \mathbf{S} \mathbf{h}_k \right) \geq \Gamma_k^{\text{th}} \left( \delta_c |\mathbf{f}_0^H \mathbf{w}_c|^2 + \delta_p \sum_{j \in \mathcal{L}} |\mathbf{f}_0^H \mathbf{w}_j|^2 + \delta_c \mathbf{f}_0^H \mathbf{S} \mathbf{f}_0 \right. \\ \left. + \sum_{i \in \mathcal{K}_k} \alpha_i \left( |\mathbf{h}_i^H \mathbf{w}_c|^2 + \sum_{j \in \mathcal{L}} |\mathbf{h}_i^H \mathbf{w}_j|^2 + \mathbf{h}_i^H \mathbf{S} \mathbf{h}_i \right) + \sigma^2 \right) + t_1, \quad \forall k, \quad (31c)$$

$$|\mathbf{f}_l^H \mathbf{w}_c|^2 \geq \tilde{\Gamma}_{c,l}^{\text{th}} \left( \sum_{j \in \mathcal{L}} |\mathbf{f}_l^H \mathbf{w}_j|^2 + \delta_s |\mathbf{f}_l^H \mathbf{s}|^2 + \sum_{k \in \mathcal{K}} \alpha_k \left( |\mathbf{h}_{l,k}^H \mathbf{w}_c|^2 + \sum_{j \in \mathcal{L}} |\mathbf{h}_{l,k}^H \mathbf{w}_j|^2 + |\mathbf{h}_{l,k}^H \mathbf{s}|^2 \right) + \sigma^2 \right), \quad \forall l, \quad (31d)$$

$$|\mathbf{f}_l^H \mathbf{w}_l|^2 \geq \tilde{\Gamma}_{p,l}^{\text{th}} \left( \delta_c |\mathbf{f}_l^H \mathbf{w}_c|^2 + \sum_{j \in \mathcal{L}_l} |\mathbf{f}_l^H \mathbf{w}_j|^2 + \delta_s |\mathbf{f}_l^H \mathbf{s}|^2 + \sum_{k \in \mathcal{K}} \alpha_k \left( |\mathbf{h}_{l,k}^H \mathbf{w}_c|^2 + \sum_{j \in \mathcal{L}} |\mathbf{h}_{l,k}^H \mathbf{w}_j|^2 + |\mathbf{h}_{l,k}^H \mathbf{s}|^2 \right) + \sigma^2 \right), \quad \forall l, \quad (31e)$$

$$(1 - \alpha_k) p_k^{\text{in}} \geq \Phi^{-1}(p_b) + t_2, \quad \forall k, \quad (31f)$$

$$0 < \alpha_k < 1, \quad \forall k, \quad (31g)$$

need complexity of  $\mathcal{O}(KN^2)$ . The total complexity for this problem is thus  $\mathcal{O}(KN^2 + N^3)$ .

2) *Optimization over  $\{\mathbf{w}_c, \mathbf{w}_l, \mathbf{S}, C_l\}$* : This SDR sub-problem is tackled using SDP, specifically the interior-point method. From [43, Th. 3.12], the order of computational complexity for a SDP problem with  $m$  SDP constraints with an  $n \times n$  positive semi-definite (PSD) matrix is given by  $\mathcal{O}(\sqrt{n} \log(1/\epsilon)(mn^3 + m^2n^2 + m^3))$ , where  $\epsilon > 0$  is the solution accuracy. In our proposed problem,  $\mathbf{P}_w$  (22),  $n = M$  and  $m = 3(K + L) + 2$ , and the approximate computational complexity is  $\mathcal{O}((K + L)M^3 \sqrt{M} \log(1/\epsilon))$ .

3) *Optimization over  $\alpha_k$* : The difference of convex (d.c.) method and the interior point method are employed [23]. The number of iterations for convergence is given by  $\frac{(\log(C)/t^0 \delta)}{\log \epsilon}$ , where  $C$  is the overall number of constraints,  $t^0$  signifies the initial approximation for the interior point method's accuracy, and  $0 < \delta \ll 1$  is the stopping criterion [40].

4) *Algorithm 1*: Finally, the proposed Algorithm 1's computational complexity can be expressed asymptotically as  $\mathcal{O}\left(I_o \left( (K + N)N^2 + (K + L)M^3 \sqrt{M} \log\left(\frac{1}{\epsilon}\right) + \frac{(\log(C)/t^0 \delta)}{\log \epsilon} \right)\right)$  where  $I_o$  is the overall number of iterations for the Algorithm 1 to converge. Despite its higher-order polynomial time complexity, the suggested approach exhibits noteworthy real-world performance for datasets up to a certain size, particularly when  $N$  and  $M$  are kept below a predefined threshold. For large datasets, adopting optimization measures such as parallel processing can dramatically enhance performance [44].

## VI. SIMULATION RESULTS

Next, simulation results are presented to assess the performance of the proposed ISABC network. The 3GPP urban micro (UMi) model is chosen to depict the path-loss values  $\zeta_a, \zeta_b$ , operating at a frequency of  $f_c = 3$  GHz [45, Table

TABLE II: Simulation parameters.

Parameter	Value	Parameter	Value
$f_c$	3 GHz	$\mathcal{R}_{t,k}^{\text{th}}$	1 bps/Hz
$B$	10 MHz	$\{\mathcal{R}_{c,l}^{\text{th}}, \mathcal{R}_{p,k}^{\text{th}}\}$	2 bps/Hz
$N_f$	10 dB	$K_{\text{SI}}$	3 dB
$M = N$	8	$\beta$	-90 dB
$L$	3	$\{\delta_c, \delta_p, \delta_s\}$	-10 dB
$K$	2	$p_b$	-20 dBm
$\mathcal{R}_{s,k}^{\text{th}}$	1 bps/Hz	$\epsilon$	$10^{-3}$

B.1.2.1]. Additionally, the AWGN variance, symbolized as  $\sigma^2$ , is modeled as  $\sigma^2 = 10 \log_{10}(N_0 B N_f)$  dBm. In this equation,  $N_0$  is given by -174 dBm/Hz, while  $B$  represents the bandwidth, and  $N_f$  denotes the noise figure. Table II lists the main simulation parameters unless mentioned otherwise. All simulations are evaluated for  $10^3$  iterations.

Considering smart home/city scenarios, the BS and the mobile reader are positioned at coordinates  $\{0, 0\}$  and  $\{12, 0\}$ , respectively. Meanwhile, tags are sporadically placed within a circle whose center is  $\{6, -4\}$  and which has a radius of 3 m [46]. Furthermore, the users are randomly scattered within a circle with a radius of 5 m and a center of  $\{55, 0\}$ .

For comparative evaluation purposes, the following benchmark schemes are considered:

1) *NOMA-assisted ISABC*: This benchmark uses NOMA to serve the primary users. For a fair comparison, BackCom and sensing at the BS are also considered, i.e.,  $\mathbf{x} = \sum_{j \in \mathcal{L}} \mathbf{w}_j x_j + \mathbf{s}$ . Without loss of generality, the channel gains are sorted in descending order, i.e.,  $\|\mathbf{f}_1\|^2 \geq \dots \geq \|\mathbf{f}_L\|^2$ . Thus,  $U_l$  first decodes the data for users with high channel gains and applies SIC before decoding its data signal. The SINR of  $U_l$  with NOMA is given in (32), where  $\mathcal{L}'_l \triangleq \{1, \dots, l-1\}$  and  $\mathcal{L}''_l \triangleq \{l+1, \dots, L\}$ . Moreover, the tags' SINRs and sensing SINRs can be easily derived by removing the common beamforming in (14) and (16), respectively. This benchmark

$$\gamma_l = \frac{|\mathbf{f}_l^H \mathbf{w}_l|^2}{\delta_p \sum_{j \in \mathcal{L}'_l} |\mathbf{f}_l^H \mathbf{w}_j|^2 + \sum_{j \in \mathcal{L}'_l} |\mathbf{f}_l^H \mathbf{w}_j|^2 + \delta_s |\mathbf{f}_l^H \mathbf{s}|^2 + \sum_{k \in \mathcal{K}} \alpha_k \left( \sum_{j \in \mathcal{L}} |\mathbf{h}_{l,k}^H \mathbf{w}_j|^2 + |\mathbf{h}_{l,k}^H \mathbf{s}|^2 \right) + \sigma^2} \quad (32)$$

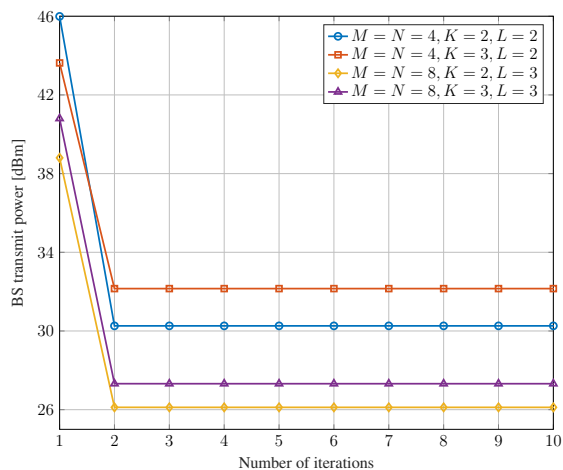


Fig. 2: Convergence of the proposed Algorithm 1.

facilitates the investigation of the impacts of RSMA compared to conventional NOMA.

2) *RSMA-assisted BackCom*: This benchmark considers multiple RSMA-enabled primary users and multiple tags. However, the BS has no sensing capabilities, i.e.,  $\mathbf{x} = \mathbf{w}_c x_c + \sum_{j \in \mathcal{L}} \mathbf{w}_j x_j$ . This benchmark helps to evaluate the cost of adding sensing.

3) *Conventional BackCom*: This benchmark considers a conventional AmBC system with  $K$ -tags and  $L$ -users. Specifically, the BS does not perform rate-splitting and sensing and uses SDMA to serve the users. Thus, the BS transmit signal becomes  $\mathbf{x} = \sum_{j \in \mathcal{L}} \mathbf{w}_j x_j$ . These tags operate solely on EH and send data to the reader by reflecting  $\mathbf{x}$ . This benchmark helps to evaluate the cost of incorporating sensing and rate-splitting.

4) *Conventional ISABC*: This benchmark uses SDMA to serve the primary users. The BS senses environmental information from  $K$  tags. Thus, the BS transmit signal becomes  $\mathbf{x} = \sum_{j \in \mathcal{L}} \mathbf{w}_j x_j + \mathbf{s}$ . The benchmark helps to gauge the difference between SDMA and RSMA.

5) *Sensing-only scheme*: This benchmark scheme evaluates a system with  $K$ -targets/tags without primary and backscatter communications. The targets/tags use EH, allowing for a fair comparison. For example, targets may be wireless sensors/tags that do not send data but harvest energy to remain active.

These benchmark schemes are special cases of Algorithm 1, which can easily handle them with minor modifications.

#### A. Convergence Rate of Algorithm 1

Algorithm 1 outputs all variable set  $\mathcal{A}$  in several iterations. Thus, the saturation of the BS transmit power is a convergence test, and Fig. 2 thus plots it as a function of the number of iterations. The stopping criterion is that the normalized objective function increases less than  $\epsilon = 10^{-3}$ . The BS

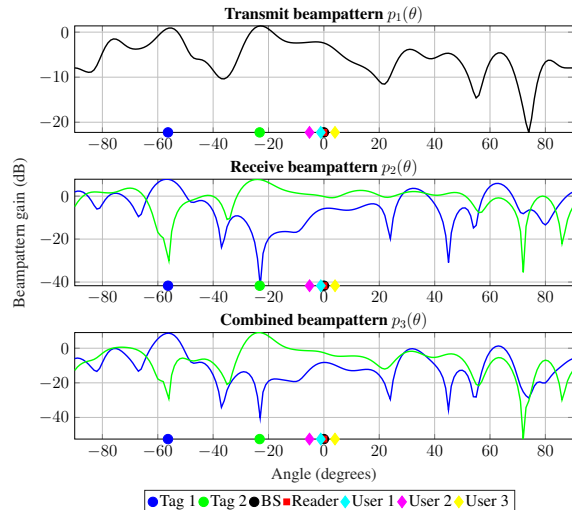


Fig. 3: Beampattern of radar functionality of Algorithm 1.

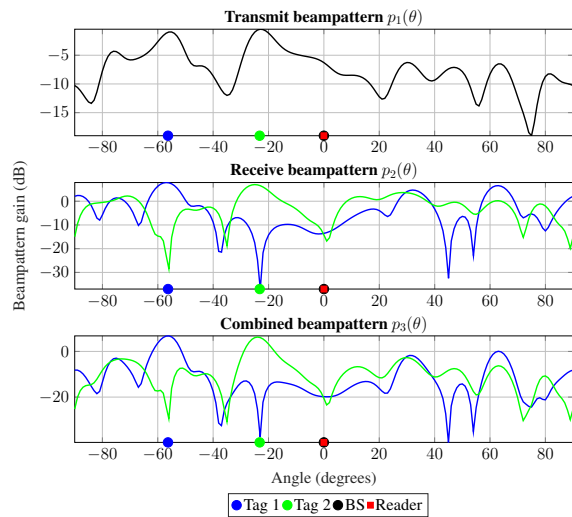


Fig. 4: Beampattern of radar functionality of sensing-only scheme.

transmit power decreases rapidly with each iteration and saturates after approximately three iterations, regardless of  $M$ ,  $L$ , or  $K$ . This implies quick convergence and validates the proposed algorithm's effectiveness. Extensive simulations reveal that Algorithm 1 requires only three iterations to attain adequate performance with any system setup, hardly improving performance beyond three iterations.

#### B. Beampattern Gains

The direct transmission and reception of beams in precise directions help to extract more information. To this end, Algorithm 1 functions as a linchpin, controlling the formation and direction of these beams. Beamforming refers to merging signals from an array of antennas to produce a directed "beam" or "lobe." This beam can be electronically steered while

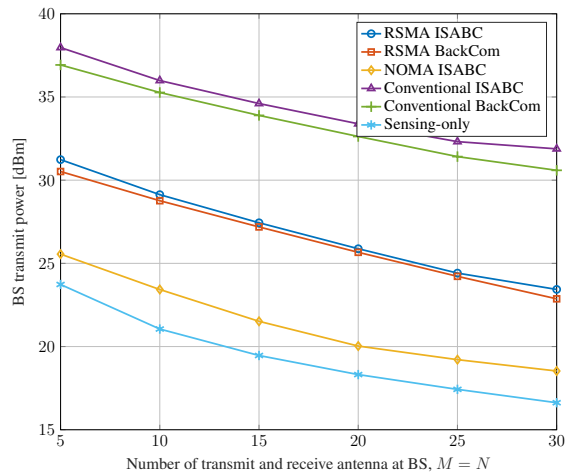


Fig. 5: BS transmit power versus the number of BS transmit/receive antennas,  $M = N$ .

the antennas stay stationary. This steering feature improves signal quality, increases backscatter tag detection, and reduces possible interference significantly.

The BS transmit signal,  $\mathbf{x}$ , represents the outward-projected energy to illuminate the targets. The received beamformer is designed for clear reception, catching echoes or reflections off the backscatter tags. The three crucial beampatterns are

$$p_1(\theta) = |\mathbf{b}^H(\theta_k)\mathbf{x}^*|^2, \quad (33a)$$

$$p_2(\theta) = |(\mathbf{u}_k^*)^H \mathbf{b}(\theta_k)|^2, \quad (33b)$$

$$p_3(\theta) = |(\mathbf{u}_k^*)^H \mathbf{b}(\theta_k) \mathbf{b}^H(\theta_k) \mathbf{x}^*|^2. \quad (33c)$$

Here, (33a) indicates how transmitted energy disperses as a function of angle  $\theta$ , while (33b) captures the sensitivity across multiple angles while receiving reflected energy. Moreover, (33c) provides a composite representation incorporating the impacts of transmission and subsequent reflection processing.

Fig. 3 and Fig. 4 illustrate the aforementioned three beampatterns generated using Algorithm 1 and the sensing-only approach, respectively. The first sub-figure in Fig. 3 shows that Algorithm 1 aims the transmit beams at tags and users. In contrast, the second sub-figure depicts the directions of interference from other tags for a specific tag with relatively deep nulls, separating the individual sensing information at the BS. The overall beampattern (third sub-figure) combines the transmit and receive beampatterns. Compared to the sensing-only scheme (Fig. 4), Algorithm 1 additionally provides users with communication capabilities while alleviating interference between targets/tags for sensing.

Fig. 3 and Fig. 4 help sense operations as they depict the radar/beampatterns. These figures offer a practical perspective, helping to better understand the intricacies and efficacy of beamforming algorithms.

### C. Effects of Number of BS Antennas

Fig. 5 and Fig. 6 show the influence of the number of BS antennas,  $M = N$ , on the BS transmit power and primary user rates, respectively. Fig. 5 shows that increasing  $M$  has an

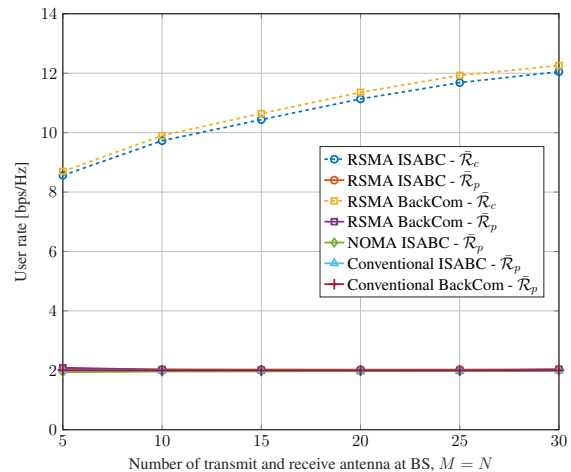


Fig. 6: Average user rate versus the number of BS transmit/receive antennas,  $M = N$ .

inverse effect on the required power. Specifically, increasing  $M$  decreases the transmit power for all the schemes. This trend suggests the spatial diversity benefits for ISABC, namely (1) increased communication rates and (2) significant power savings. Additionally, NOMA and sensing-only schemes consume the lowest amount of transmit power. This is because NOMA has no common rate requirements (i.e., constraint (17d)), and the sensing-only approach lacks communication. As a result, NOMA achieves a significantly lower user rate than RSMA (Fig 6). In contrast, conventional BackCom and ISABC consume the most power resulting from multi-user multi-tag interference. Conversely, the proposed setup and RSMA-assisted BackCom have moderate transmit power requirements. Importantly, the proposed IMBO algorithm enables sensing, a critical feature for IoT networks, with only a modest transmit power increase.

Fig. 6 compares the average primary user rates of all the schemes, i.e.,  $\bar{\mathcal{R}}_c \triangleq 1/L \sum_{l \in \mathcal{L}} \mathcal{R}_{c,l}$  and  $\bar{\mathcal{R}}_p \triangleq 1/L \sum_{l \in \mathcal{L}} \mathcal{R}_{p,l}$ . The figure shows the proposed scheme achieves the highest communication rate among all. The reason is that RSMA enables the optimization of the common rates, which increases them. For example, just for a 24% transmit power increase ( $M = N = 10$ ), our scheme achieves a 350% rate gain over NOMA-assisted ISABC.

### D. Transmit Power Versus Number of Tags

Fig. 7 exhibits the intricate relationship between the number of tags and the BS transmit power requirements. From Fig. 7, these two variables show an evident linear correlation across all schemes. Although the NOMA and sensing-only methods reduce the transmit power, they also have inferior communication performance (Fig. 6).

Conversely, both conventional BackCom and conventional ISABC demand higher BS transmit power to satisfy communication (and/or sensing) rates and EH while mitigating multi-user multi-tag interference. In contrast, both the proposed and RSMA-assisted BackCom utilize a moderate BS transmit power. Nonetheless, compared to RSMA-assisted BackCom,

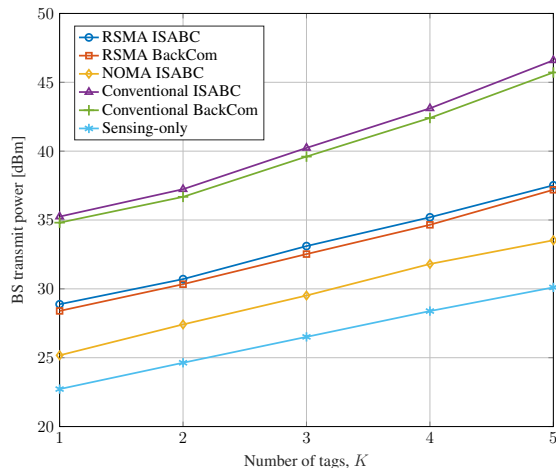


Fig. 7: Transmit power versus the number of tags,  $K$ .

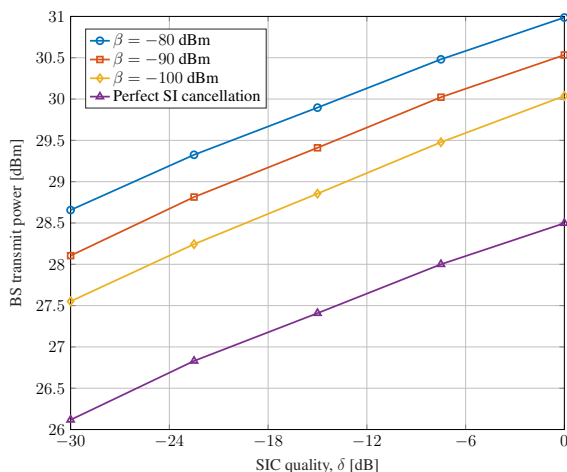


Fig. 8: Transmit power versus SIC imperfection  $\delta$  for various residual SI values.

the proposed ISABC approach requires a low power increase and promotes both communication and sensing by transforming passive tags into proactive participants.

### E. Impacts of SIC and SI cancellation

Impairments, such as SIC errors and SI cancellation quality, can degrade the performance and reliability. SIC errors harm signal reception and detection. SI cancellation errors occur when FD nodes cannot fully remove SI, hindering incoming signal reception. Both errors have a significant impact.

Fig. 8 examines the effects of imperfect SIC and SI cancellation on Algorithm 1. The BS transmit power is plotted as a function of SIC quality, i.e.,  $\delta = \delta_c = \delta_p = \delta_s$ , for various SI cancellation qualities, i.e.,  $\beta = \{-80, -90, -100\}$  dB and perfect SI cancellation, at the BS.

According to Fig. 8, severe SIC imperfection, i.e.,  $\delta \rightarrow 1$  (0 dB) requires the BS to transmit additional power to alleviate the adverse effects of SIC imperfection while maintaining tag EH requirements and communication/sensing rates. Conversely, when  $\delta \rightarrow 0$  or perfect SIC, less power is

required to sustain these demands. Imperfect SI cancellation has bad consequences. Variable  $\beta \in [0, 1]$  reflects the degree of imperfection at the BS. Further experiments offer insight into transmission power with varying residual SI values. Like SIC errors, the BS transmit power is sacrificed as  $\beta$  increases.

## VII. CONCLUSION

This paper presents a novel framework integrating RSMA and ISABC into a cohesive system. Within this framework, the FD BS assumes dual functionality: first, it acts as a sensor to detect information from backscatter tags, and second, it employs RSMA for efficient communication with multiple users. Conversely, the backscatter reader is responsible for detecting multi-tag backscatter data.

An advanced AO-based algorithm is introduced to precisely regulate communication channels, both primary and backscatter, while concurrently reducing the transmit power of the BS. This innovation facilitates passive tags' opportunistic sensing and communication within forthcoming IoT networks. To evaluate its performance, the proposed system is benchmarked against NOMA and SDMA, as well as sensing-only and communication-only approaches.

Through rigorous comparison, the RSMA-based system demonstrates significant advantages over NOMA and SDMA counterparts. Furthermore, the study delves into the impact analysis of SIC errors and the quality of SI cancellation. Looking ahead, numerous avenues for future research emerge, particularly machine learning techniques tailored for channel estimation and interference mitigation within ISABC systems.

## APPENDIX A PROOF OF THEOREM 1

The main problem is divided into three sub-problems, which optimize tag reflections coefficients ( $\alpha := \{\alpha_k\}_{k \in \mathcal{K}}$ ), received beamforming ( $\mathbf{U} := \{\mathbf{u}_k\}_{k \in \mathcal{K}}$ ), and transmit beamforming ( $\mathbf{P} = \{\mathbf{w}_c, \{\mathbf{w}_l\}_{l \in \mathcal{L}}, \mathbf{S}, \{C_l\}_{l \in \mathcal{L}}\}$ ), via solving problems (21), (30), and (31), while keeping the other two blocks of variables fixed. Let us define  $F(\mathbf{U}, \alpha, \mathbf{P})$  as a function of  $\mathbf{U}$ ,  $\alpha$ , and  $\mathbf{P}$  for the objective value of (17a). First, in step 3 of Algorithm 1 with fixed variables  $\alpha^{(i)}$  and  $\mathbf{P}^{(i)}$ ,  $\mathbf{U}^{(i+1)}$  is the optimal solution that minimizes the value of the objective function. Accordingly, the following holds:

$$F(\alpha^{(i)}, \mathbf{U}^{(i+1)}, \mathbf{P}^{(i)}) \leq F(\alpha^{(i)}, \mathbf{U}^{(i)}, \mathbf{P}^{(i)}). \quad (34)$$

Next, in step 4 of Algorithm 1,  $\mathbf{P}^{(i+1)}$  is the optimal transmit beamformers with given variables  $\alpha^{(i)}$  and  $\mathbf{U}^{(i+1)}$  to minimize  $F$  via solving (22a). Thus, it guarantees that

$$F(\alpha^{(i)}, \mathbf{U}^{(i+1)}, \mathbf{P}^{(i+1)}) \leq F(\alpha^{(i)}, \mathbf{U}^{(i+1)}, \mathbf{P}^{(i)}). \quad (35)$$

Finally, in step 5 of Algorithm 1 with the given  $\mathbf{P}^{(i+1)}$  and  $\mathbf{U}^{(i+1)}$ , problem (30) is solved to obtain an optimal solution for  $\alpha^{(i)}$ , which yields:

$$F(\alpha^{(i+1)}, \mathbf{U}^{(i+1)}, \mathbf{P}^{(i+1)}) \leq F(\alpha^{(i)}, \mathbf{U}^{(i+1)}, \mathbf{P}^{(i+1)}). \quad (36)$$

According to (34)–(36), it follows that

$$F(\alpha^{(i+1)}, \mathbf{U}^{(i+1)}, \mathbf{P}^{(i+1)}) \leq F(\alpha^{(i+1)}, \mathbf{U}^{(i+1)}, \mathbf{P}^{(i+1)}). \quad (37)$$

The objective values of Algorithm 1 monotonically decrease with each iteration, always remaining non-negative. This consistency, combined with the design choice where each iteration starts from the previous one's end, ensures the algorithm's convergence. Thus, the proof is completed.

## REFERENCES

- [1] "3GPP TR 22.837, Feasibility study on integrated sensing and communication, V.19.3.0 Rel. 19," Apr. 2024. [Online]. Available: <https://portal.3gpp.org/desktopmodules/Specifications/SpecificationDetails.aspx?specificationId=4044>
- [2] D. T. Hoang, D. Niyato, D. I. Kim, N. V. Huynh, and S. Gong, *Ambient Backscatter Communication Networks*. Cambridge University Press, 2020.
- [3] D. Galappaththige, F. Rezaei, C. Tellambura, and S. Herath, "Link budget analysis for backscatter-based passive IoT," *IEEE Access*, vol. 10, pp. 128 890–128 922, Dec. 2022.
- [4] F. Rezaei, D. Galappaththige, C. Tellambura, and S. Herath, "Coding techniques for backscatter communications - A contemporary survey," *IEEE Commun. Surveys Tuts.*, pp. 1020–1058, 2th Quart. 2023.
- [5] F. Rezaei, C. Tellambura, and S. Herath, "Large-scale wireless-powered networks with backscatter communications—A comprehensive survey," *IEEE Open J. Commun. Soc.*, vol. 1, pp. 1100–1130, Aug. 2020.
- [6] D. Galappaththige, C. Tellambura, and A. Maaref, "Integrated sensing and backscatter communication," *IEEE Wireless Commun. Lett.*, vol. 12, no. 12, pp. 2043–2047, Dec. 2023.
- [7] S. Zargari, D. Galappaththige, and C. Tellambura, "Transmit power optimization for integrated sensing and backscatter communication," *arXiv*, 2024.
- [8] "3GPP TSG RAN –97e3, Study on ambient IoT , 9.1 (from RP-222685)," Sept. 2022. [Online]. Available: <https://portal.3gpp.org/ngppapp/TdocList.aspx?meetingId=60043>
- [9] "3GPP TSG RAN Meeting –94e, Study proposal on passive IoT, 8A.1 (from RP-213368)," Dec. 2021. [Online]. Available: <https://www.3gpp.org/DynaReport/TDocExMtg--RP-94-e--60214.htm>
- [10] W. U. Khan, F. Jameel, N. Kumar, R. Jäntti, and M. Guizani, "Backscatter-enabled efficient V2X communication with non-orthogonal multiple access," *IEEE Trans. Veh. Technol.*, vol. 70, no. 2, pp. 1724–1735, Feb. 2021.
- [11] Y. Xu *et al.*, "Robust resource allocation for wireless-powered backscatter communication systems with NOMA," *IEEE Trans. Veh. Technol.*, vol. 72, no. 9, pp. 12 288–12 299, Sept. 2023.
- [12] A. Liu *et al.*, "A survey on fundamental limits of integrated sensing and communication," *IEEE Commun. Surveys Tuts.*, vol. 24, no. 2, pp. 994–1034, 2th Quart. 2022.
- [13] Z. He *et al.*, "Full-duplex communication for ISAC: Joint beamforming and power optimization," *IEEE J. Sel. Areas Commun.*, vol. 41, no. 9, pp. 2920–2936, Sept. 2023.
- [14] M. Mohammadi, Z. Mobini, D. Galappaththige, and C. Tellambura, "A comprehensive survey on full-duplex communication: Current solutions, future trends, and open issues," *IEEE Commun. Surveys Tuts.*, vol. 25, no. 4, pp. 2190–2244, 4th Quart. 2023.
- [15] B. Clerckx, H. Joudeh, C. Hao, M. Dai, and B. Rassouli, "Rate splitting for MIMO wireless networks: A promising PHY-layer strategy for LTE evolution," *IEEE Commun. Mag.*, vol. 54, no. 5, pp. 98–105, May 2016.
- [16] Y. Mao *et al.*, "Rate-splitting multiple access: Fundamentals, survey, and future research trends," *IEEE Commun. Surveys Tuts.*, vol. 24, no. 4, pp. 2073–2126, 2th Quart. 2022.
- [17] C. Xu, B. Clerckx, S. Chen, Y. Mao, and J. Zhang, "Rate-splitting multiple access for multi-antenna joint radar and communications," *IEEE J. Sel. Topics Signal Process.*, vol. 15, no. 6, pp. 1332–1347, Nov. 2021.
- [18] Y. Mao, B. Clerckx, and V. O. Li, "Rate-splitting multiple access for downlink communication systems: Bridging, generalizing, and outperforming sdma and NOMA," *EURASIP J. Wireless Commun. Netw.*, vol. 2018, pp. 1–54, Dec. 2018.
- [19] R. Long, Y.-C. Liang, H. Guo, G. Yang, and R. Zhang, "Symbiotic radio: A new communication paradigm for passive internet of things," *IEEE Internet Things J.*, vol. 7, no. 2, pp. 1350–1363, Feb. 2020.
- [20] J. C. Bezdek and R. J. Hathaway, "Convergence of alternating optimization," *Neural, Parallel & Scientific Computations*, vol. 11, no. 4, pp. 351–368, Dec. 2003.
- [21] A. M.-C. So, J. Zhang, and Y. Ye, "On approximating complex quadratic optimization problems via semidefinite programming relaxations," *Mathematical Programming*, vol. 110, no. 1, pp. 93–110, Jun. 2007.
- [22] Q. Wu and R. Zhang, "Intelligent reflecting surface enhanced wireless network via joint active and passive beamforming," *IEEE Trans. Wireless Commun.*, vol. 18, no. 11, pp. 5394–5409, Nov. 2019.
- [23] S. Zargari, S. Farahmand, B. Abolhassani, and C. Tellambura, "Robust active and passive beamformer design for IRS-aided downlink MISO PS-SWIPT with a nonlinear energy harvesting model," *IEEE Trans. Green Commun. Netw.*, vol. 5, no. 4, pp. 2027–2041, Dec. 2021.
- [24] M. Razaviyayn, M. Hong, and Z.-Q. Luo, "A unified convergence analysis of block successive minimization methods for nonsmooth optimization," *SIAM J. Optim.*, vol. 23, no. 2, pp. 1126–1153, Sept. 2013.
- [25] "Positioning techniques for mobile devices in LTE," July 2015. Available Online: <https://www.hsc.com/resources/blog/positioning-techniques-for-mobile-devices-in-lte/>
- [26] T. Kim, K. Min, and S. Park, "Self-interference channel training for full-duplex massive MIMO systems," *Sensors*, vol. 21, no. 9, p. 3250, May 2021.
- [27] Y. Zhang, Q. Zhang, Y.-C. Liang, and P. Y. Kam, "A semi-blind receiver for ambient backscatter communications with MPSK RF source," in *IEEE/CIC Int. Conf. Commun. Workshops China (ICCC Workshops)*, Aug. 2019, pp. 71–76.
- [28] S. Zargari, A. Hakimi, C. Tellambura, and A. Maaref, "Enhancing AmBC systems with deep learning for joint channel estimation and signal detection," *IEEE Trans. Commun.*, pp. 1–1, 2023.
- [29] F. Rezaei, D. Galappaththige, C. Tellambura, and A. Maaref, "Time-spread pilot-based channel estimation for backscatter networks," *IEEE Trans. Commun.*, vol. 72, no. 1, pp. 434–449, Jan. 2024.
- [30] Y. Liao, G. Yang, and Y.-C. Liang, "Resource allocation in NOMA-enhanced full-duplex symbiotic radio networks," *IEEE Access*, vol. 8, pp. 22 709–22 720, Jan. 2020.
- [31] R. Zhang and C. K. Ho, "MIMO broadcasting for simultaneous wireless information and power transfer," *IEEE Trans. Wireless Commun.*, vol. 12, no. 5, pp. 1989–2001, May 2013.
- [32] A. Hakimi, S. Zargari, C. Tellambura, and S. Herath, "Sum rate maximization of MIMO monostatic backscatter networks by suppressing residual self-interference," *IEEE Trans. Commun.*, vol. 71, no. 1, pp. 512–526, Jan. 2023.
- [33] E. Boshkovska, D. W. K. Ng, N. Zlatanov, and R. Schober, "Practical non-linear energy harvesting model and resource allocation for SWIPT systems," *IEEE Commun. Lett.*, vol. 19, no. 12, pp. 2082–2085, Dec. 2015.
- [34] Z. He, W. Xu, H. Shen, Y. Huang, and H. Xiao, "Energy efficient beamforming optimization for integrated sensing and communication," *IEEE Wireless Commun. Lett.*, vol. 11, no. 7, pp. 1374–1378, Jul. 2022.
- [35] P. Stoica, J. Li, and Y. Xie, "On probing signal design for MIMO radar," *IEEE Trans. Signal Process.*, vol. 55, no. 8, pp. 4151–4161, Aug. 2007.
- [36] G. Cui, H. Li, and M. Rangaswamy, "MIMO radar waveform design with constant modulus and similarity constraints," *IEEE Trans. Signal Process.*, vol. 62, no. 2, pp. 343–353, Jan. 2014.
- [37] D. P. Bertsekas, "Nonlinear Programming," *J. Oper. Res. Soc.*, vol. 48, no. 3, pp. 334–334, 1997.
- [38] S. Stanczak, *Fundamentals of Resource Allocation in Wireless Networks Theory and Algorithms*, 2nd ed. Berlin, Heidelberg: Springer Berlin Heidelberg, 2008.
- [39] W. Wan, X. Wang, J. Yang, and B. Zhao, "Joint linear pre-coder and combiner optimization for distributed antenna systems," in *IEEE Global Commun. Conf. (GLOBECOM)*, Dec. 2016, pp. 1–6.
- [40] S. Boyd and L. Vandenberghe, *Convex Optimization*. Cambridge, U.K.: Cambridge Univ. Press, Mar. 2004.
- [41] M. Grant and S. Boyd, "CVX: Matlab software for disciplined convex programming, version 2.1," 2014.
- [42] K. Shen and W. Yu, "Fractional programming for communication systems—part I: Power control and beamforming," *IEEE Trans. Signal Process.*, vol. 66, no. 10, pp. 2616–2630, May 2018.
- [43] I. P'olik and T. Terlaky, *Interior Point Methods for Nonlinear Optimization*. Berlin, Germany; New York, NY, USA: Springer, 2010.
- [44] C. E. Leiserson and T. B. Schardl, "A work-efficient parallel breadth-first search algorithm (or how to cope with the nondeterminism of reducers)," in *Proc. 22nd ACM symp. Parallelism in Algorithms and Archit.*, Jun. 2010, pp. 303–314.
- [45] "3GPP TR 36.814, Further advancements for E-UTRA physical layer aspects, V.9.0.0 Rel. 9," Mar. 2010. [Online]. Available: <https://portal.3gpp.org/desktopmodules/Specifications/SpecificationDetails.aspx?specificationId=4044>
- [46] D. Galappaththige, F. Rezaei, C. Tellambura, and S. Herath, "RIS-empowered ambient backscatter communication systems," *IEEE Wireless Commun. Lett.*, vol. 12, no. 1, pp. 173–177, Jan. 2023.